Supporting Information

Choi et al. 10.1073/pnas.1314209111

SI Text Overview

This report identifies key molecular regulatory events affecting conformation and membrane distribution of individual β1 integrin molecules controlled by plexinD1 and sema3E during thymocyte development. We show that the plexinD1 and sema3E regulation of β1 integrin spatial arrangement and catch bond stability contributes to the fine tuning of thymocyte chemokine-driven migration during development and that disturbance of this pathway leads to defects in negative selection and autoimmune phenomena.

The key cellular event underlying the role of plexinD1 in thymocyte development was identified previously as the inability of positively selected double-positive (DP) thymocytes to continue their programmed developmental migration from the cortex to the medulla in the absence of plexinD1 (1). To dissect the underlying mechanism, we had to consider some of the main controls on migratory behavior, these being capacity to respond to chemokines, with consequent appropriate migration, and cellular adhesion molecule dynamics permitting adhesion at the leading edge and detachment at the trailing edge. We had to consider pathways downstream of chemokine receptors influencing adhesion, as well as alterations in adhesion receptor surface expression, conformational states influencing activation and adhesion, and recycling of adhesion molecules from the membrane by endocytosis.

To address these issues, we created *Plxnd1*$^{flox/flox}$ pLckCre transgenic (D1CKO) mice. By placing the Cre under the control of a T lineage–specific promoter, *Plxnd1* is conditionally knocked out only during T-cell development in the thymus and plexinD1 is not expressed on developing T cells at any stage subsequent to the DN compartment (DN cells even in the WT do not express plexinD1 (1) (Fig. 5*B* and Fig. S2*D*). Nevertheless, in all other developmental processes that require plexinD1, including embryonic cardiovascular and cerebral development, as well as vascular angiogenesis, plexinD1 expression is normal and appropriate. Further, in thymocytes derived from these D1CKO mice, *Plxnd1* is the only transcript significant down-regulated.

We then demonstrate that WT and D1CKO thymocytes behave identically in response to CXCL12 chemokine, indicating no aberration in ability to initiate and establish migration (Fig. 2*C*, *Upper Left*). These results have provided further insight into our initial results indicating that sema3E binding to plexinD1 may directly regulate CCL25 signaling through thymocyte surface-expressed CCR9 (1). In particular, we examined the possibility that plexinD1 was disengaging the direct connection between chemokine signaling and the cycles of adhesion and detachment necessary for directional chemokine-induced migration. To examine the effects of loss of plexinD1 upon adhesion, we focused specifically on integrins because these are the main mediators for this effect in hematopoietic cells. The DP thymocyte integrin display and its relation to that on other thymocytes has not been systematically established, so we undertook an evaluation of all α and β integrin chains on thymocyte subsets (Figs. S2–S4), as well as localization of ligand expression in the thymus (Fig. 1 and Fig. S1), allowing us to focus specifically on α4β1 interacting with VCAM-1 and α6β1 interacting with laminin as being important for DP thymocyte interactions in the thymic cortex (Fig. S2*B*). No significant difference in levels of expression of any integrin on WT and D1CKO thymocytes could be detected (Fig. S3), and no difference in the CD69 developmental activation marker consequent to positive selection was evident (Fig. S2*A*). Expression of α4 chain in an active conformation [metal ion–dependent adhesion site (MIDAS) motif exposed state] was also identical between WT and D1CKO cells (Fig. S2 *C*–*E*). Examination of pathways downstream of CXCL12 stimulation, specifically activation of Rap1/2, a focal mediator of integrin activation, revealed no difference between WT and D1CKO cells (Fig. S8*B*), and we found no evidence of any β1 integrin internalization in thymocytes following CXCL12 with or without sema3E treatment (Fig. S8*A*). To even detect the signal we observed in Fig. S8*A*, exposure had to be extended considerably and was reproducibly low in five separate experiments.

As described in the main text, we then focused on the two remaining aspects of integrin functionality that may affect avidity and, as a consequence, adhesion. Specifically, we examined alterations in the arrangement and clustering of β1 integrin on the membrane in the absence of *Plxnd1* in the D1CKO mice (Fig. 3 and Figs. S9 and S10) and possible regulation of sema3E of the β1 integrin/ligand bond itself (Fig. 3 *C*–*E* and Fig. S11). Although the adhesion data establishes an effect of plexinD1 and sema3E on adhesion under stress conditions for both α4β1 and α6β1 (Fig. 2 *A* and *B* and Fig. S7), only α4β1/VCAM-1 interaction was studied using the biomembrane force probe (BFP). Natural laminin isoforms could not be uniformly oriented on the glass bead, and recombinant laminin with a domain amenable to orientation is difficult to produce as an αβγ chain trimer placing it beyond the scope of this study. The investigative line taken here was fundamentally different to that in our initial report because we were now targeting adhesion through specific integrins to thymic-expressed substrates in contrast to simple transwell migration assays across uncoated membranes (1).

The data then clearly reveal the catch bond state of the α4β1 on thymocytes (Fig. 3*D* and Fig. S11). It is critical to note that the catch bonds are fully operating in both the WT and D1CKO thymocytes. In the latter instance, the bonds simply cannot be regulated by sema3E (Fig. 4*B*). The maintenance of these integrin catch bonds seems the most reasonable explanation for the cortical retention of *Plxnd1*$^{-/-}$ thymocytes that we previously observed (1), even if the β1 integrins are less well clustered, leading to lower avidity. The evidence for the effect of clustering on β1 integrin avidity is unequivocal. Comparison of the relative mobility of adherent WT cells on VCAM-1 under flow (Movie S3) with D1CKO cells under the same conditions (Movie S5) demonstrates the detachment and reattachment of the latter, whereas WT cells remain firmly attached. The lower avidity may afford the D1CKO cells some extra level of mobility within the cortex, but at no point will they be able to respond to the sema3E emanating from the medulla (1). Meanwhile, postselection WT CD69^{+} DP thymocytes migrating in the cortex will release their β1 integrin catch bonds on exposure to sema3E, leading to reduced interaction with cortical VCAM-1 and laminin and permitting maximal response through expressed CCR7 chemokine receptor to CCL19/CCL21, also originating from the medulla.

SI Materials and Methods

Mice. *Plxnd1*$^{flox/flox}$ pLckCre transgenic (tg), Rip-mOVA tg (2), and OTII-TCR tg (3) mice were bred and maintained under pathogen-free conditions at the Dana-Farber Cancer Institute. All of the mice were backcrossed more than 10 times onto the C57BL/6J background. All of the animal experiments were performed in accordance with the Institutional Animal Care and Use Committee of Dana-Farber Cancer Institute and Harvard Medical School.

Antibodies and Proteins. Anti-keratin8 (Troma1) Ab, sema3E-mFc, and polyclonal anti-plexinD1 Ab were purified and labeled as described previously (1). Anti-mouse mucosal addressin cell adhesion molecule 1 (MAdCAM1) (MECA-367) antibody was obtained from Biolegend. Anti-thrombospondin 1/2 (H-300) Ab, anti-Rap1 (1A/1B), and anti-Rap2 (2A/2B/2C) antibodies were obtained from Santa Cruz Biotechnology. Anti-MHCII (clone M5/114.15.2), anti-Vβ5.1/5.2 (clone MR9.4), anti-CD3ε (clone 145.2C.11), anti-B220, anti-CD69 (clone H1.2F3), anti-CD8 (clone 53.6.72), anti-CD4 (clone GK1.5), anti-VCAM1 (CD106), anti-ICAM1 (CD54), and all of the anti–α integrins and –β integrins Abs except SG31 were obtained from eBioscience. ER-TR5 antibody was provided by W. van Ewijk (Leiden University Medical Center, Leiden, The Netherlands). SG31 was a kind gift from John F. Kearney (University of Alabama, Birmingham, AL). Anti-laminin, anti-osteopontin, anti-fibronectin, UEA1-FITC, and purified laminin and collagen were obtained from Sigma-Aldrich. Anti-mouse IgG2c-PE and the biotinylated anti-human IgG-F(ab')$_2$ fragment were obtained from Jackson ImmunoResearch. Recombinant mouse VCAM1-hFc, E-cadherin-hFc, and mouse CXCL12 were obtained from R&D Systems. Anti-insulin was obtained from Cell Signaling. Anti-rabbit HRP and anti-mouse HRP were obtained from Invitrogen. GTPγS was obtained from Cytoskeleton.

Confocal Microscopy. Thymic frozen sections were analyzed as described previously (1). Briefly, following embedding in O.C.T. compound (Sakura Finetek), sectioning, and fixation in acetone for 10 min, thymic frozen sections (4 μm) were stained with the indicated antibodies after blocking in 1% BSA-TBST overnight at 4 °C. Following staining, the sections were analyzed using an LSM710 confocal laser-scanning microscope (Ar and He-Ne lasers; excitation at 488, 546, and 633 nm; Carl Zeiss MicroImaging) with a 20× dry lens or 40× oil lens. Note that in all instances, images were initially taken in monochrome for maximum resolution and subsequently digitally colored for optimum differentiation. Specific details for Fig. 1 and Fig. S1 are as follows.

Fig. 1 A and B. The tissue sections were incubated with rabbit anti–VCAM-1 or anti-laminin antibodies for 2 h at 4 °C. After three washes, bound antibody was detected using anti-rabbit IgG-TRITC, and the thymic epithelial cell network identified was using anti-keratin8 FITC. In merged images, the yellow color indicates colocalization of VCAM-1 and keratin8 on cortical thymic epithelial cells (cTECs) alone, whereas laminin colocalizes with both cTECs and medullary TECs (mTECs).

Fig. 1C. Following staining with anti-ICAM1 FITC, anti–MHCII-APC, and anti-keratin8 TRITC, the keratin8 and MHCII colocalize (cyan in merged image) marking TECs, whereas the ICAM1 signal is dominantly expressed on mTECs (yellow/white color). Following staining with anti-CD8 TRITC, anti-CD4 FITC, and anti–MHCII-APC, in the merged image, the yellow color in the cortex indicates CD4$^+$CD8$^+$ coexpression on DP thymocytes, whereas in the medulla, single-positive (SP) red and green cells localize with the MHCII strongly expressed therein (blue). Following incubation with ER-TR5 (rat IgM isotype mAb marking thymic medulla) and anti-osteopontin antibodies and washing three times, the section was stained with anti-rat IgM–Alexa-fluor-647 and anti-rabbit IgG-TRITC and UEA1-FITC (also marking thymic medulla). In the merged image, the osteopontin signal colocalizes well with the ER-TR5 signal (yellow color) but not with the UEA1 signal (blue/purple color).

Fig. 1D. Following incubation with anti–MAdCAM1-biotin, the section was stained with streptavidin FITC, anti-CD8 TRITC, and anti–CD4-APC. In the merged image, the yellow region indicates cortical colocalization of CD4 and CD8 signals. Note that, although the MAdCAM1 signal localizes to the medulla (blue), the signal is discrete from the SP population.

Following incubation with anti-fibronectin, anti-osteopontin, or anti-thrombospondin antibodies, the sections were washed and stained with anti-keratin8 TRITC, anti–MHCII-APC, and anti-rabbit IgG FITC. Both keratin8 and MHCII indicate TECs, whereas the MHCII bright area indicates the medulla. In merged images, fibronectin marked the outer thymic capsule and thymic vasculature. Osteopontin strongly localized to the medulla but not on MHCII$^+$ mTECs. In contrast, thrombospondin marked MHCII$^+$ mTECs (pale blue/cyan).

Fig. S1. To identify which cell type expresses osteopontin, thymic sections were stained with the indicated antibody combinations. In the CD4$^+$ (green)/CD8$^+$ (red) merged image, the yellow region indicates the cortex, and the green region indicates medulla. Osteopontin localized to the medulla but not with CD4 SP or CD8 SP cells. In the merged image of MHCII/keratin8 signals (yellow), osteopontin was found in the MHCII^{hi} medulla but did not colocalize specifically with either the keratin8 or MHCII signal. In the merged image of UEA1 and ER-TR5 signals, the osteopontin fluorescence colocalized with ER-TR5 signal (yellow) but not with UEA1 signal (blue).

For plexinD1 and β1 integrin colocalization analysis, 10^6 thymocytes (from C57BL/6J mice) were incubated with the indicated reagents (sema3E-Fc at 5 μg/mL or phorbol ester at 10 ng/mL or CXCL12 at 200 ng/mL, respectively) for 30 min on ice and then were stimulated by incubating at 37 °C for 30 min. After washing twice with ice cold PBS, the cells were incubated again with sema3E-Fc (5 μg/mL) for 30 min on ice to saturate surface plexinD1. After a further wash with ice-cold PBS, the cells were stained for 30 min on ice with anti–β1 integrin mAb FITC (1 μg/mL) and anti-mouse IgG TRITC (1 μg/mL) to detect surface sema3E-Fc. After washing and fixation with 4% paraformaldehyde in PBS for 30 min on ice, the cells were spun down onto poly-L-lysine–coated coverslips at 800 × *g* for 15 s and mounted in antifade mounting medium with DAPI (Santa Cruz Biotechnology) on glass slides. Images were taken using a 63× oil lens. In the merged images, green color indicates integrins, red color indicates plexinD1, and yellow color indicates the colocalization between the integrin and plexinD1.

Flow Cytometry. Cells were stained with the indicated fluorescent dye-labeled mAbs or Fc-fusion proteins and subsequently stained with fluorescent-labeled secondary reagents as described previously (1). For activated α4 integrin detection, the cells were stained first with SG31, followed by anti-rat IgG-Alexa Fluor 647. After washing, the cells were stained with other mAbs as described above.

Chemotaxis and Cell Motility Imaging. Single cell suspensions of primary thymocytes from the indicated mice were resuspended in RPMI-1640 medium (10^6/mL). Unfractionated thymocytes were examined in individual experiments unless otherwise stated to minimize the potential effects of experimental manipulations on cell function. The DP subset represents ~85% of thymocytes in WT B6 and D1CKO thymii, where more than 90% of the DP cells express plexinD1 and bind sema3E (1) (Fig. 3*C*). At the phenotypic level, we observe no difference between levels of differentiating WT and *Plxnd1*$^{-/-}$ thymocyte subsets defined by surface phenotype (1). Fifteen microliters was loaded onto a μ-slide V channel (ibidi GmbH). Following addition of CXCL12 (0.5 μL at 2.5 μg/mL) to one side of the channel, the slide was loaded onto the objective table of a Juli microscope apparatus (NanoEnTek) maintained within a 37 °C incubator. Cell images were taken every minute for 40 min to 1 h and assembled into a video file using the manufacturer-supplied software. For cell rolling analysis, the cells were similarly loaded to that described above using the μ-slide III$^{0.1}$ or VI$^{0.1}$ channel slide (ibidi GmbH) and incubated for 20–30 min at 37 °C. Where WT cells were directly compared with D1CKO cells in the same chamber, the

D1CKO cells were prelabeled with a 2′,7′-bis-(2-carboxyethyl)-5-(and-6)-carboxyfluorescein, acetoxymethyl ester (BCECF-AM) fluorophore. Through addition of media (60 μL) to one side of the channel, flow was induced by gravity. Cell images were taken every minute for 40–70 min and assembled as described above. Individual cell motility was determined using ImageJ software incorporating the MTrackJ particle tracking plug-in (4). Adherence under static conditions was assayed as described (5). Pause times of rolling adherent cells were measured as previously described (6).

Direct Stochastic Optical Reconstruction Microscopy Imaging and Analysis. Image analysis of molecular clustering was performed using Getis and Franklin's second-order analysis as previously described (7). Raw intensity images under total internal reflection fluorescence illumination were processed with Zen 2010D (Zeiss MicroImaging) to identify the localization of single molecules by 2D Gaussian point spread function fitting. A model-based method was used to correct for stage drift. Overcounting of molecules due to repetitive switch of fluorophores between dark and bright states was prevented by grouping into single localization events that were dark for less than 900 ms after initial excitation. Events with localization precision worse than 50 nm were discarded, and the 2D molecular coordinates of the 4 × 4-μm region containing single cells were used for Ripley's K-function calculation

$$K(r) = A\sum_{i=1}^{n}\sum_{j=1}^{n}\left(\frac{\delta_{ij}}{n^2}\right) \quad \text{where} \quad \delta_{ij} = 1 \quad \text{if} \quad \delta_{ij} < r, \quad \text{else } 0, \qquad \textbf{[S1]}$$

where n is the number of points contained in a field-of-view of area A. δ_{ij} is the distance between two points i and j, where r is the analyzed spatial scale. Ripley's K-function is a measure of the number of points encircled within concentric circles of radius r centered on each point and scales with circle area. It is therefore transformed into the L-function such that scaling is linear with radius, r, via Eq. **S2**

$$L(r) = \sqrt{\frac{K(r)}{\pi}}. \qquad \textbf{[S2]}$$

Random distributions have $L(r) = r$ at all r. We therefore plot $L(r) - r$ vs. r. Positive values of $L(r) - r$ at a given r indicate clustering at that spatial scale. Points at the edge of the analyzed region were weighted to negate edge effects; 99% CIs were generated by simulating 100 spatially random distributions. $L(r)$ values at a spatial scale of 50 nm, $L(50)$, were computed for each point individually to generate a pseudocolored cluster heat map (MATLAB v4 interpolation algorithm on a 10-nm resolution grid). This map was thresholded at a value of $L(50) = 105$ to generate a binary cluster map from which cluster statistics (number, size) could be extracted.

BFP Analysis. The piconewton binding force was calculated by the BFP stiffness k_{bfp} times the displacement of the bead. To determine the BFP stiffness k_{bfp}, we measured the suction pressure and the radii of the probe pipette, the spherical portion of the RBC, and the contact area between the probe and the RBC (8–10), which was set at 0.15–0.3 pN/nm. To measure bond lifetime under a force, the target cell was programmed to approach and contact the probe bead for 0.1 s to allow for bond formation, to retract at a speed of 3 μm/s, to hold at a desired force (force-clamp) (Fig. S13) for lifetime measurement, and then to return to the original position to wait for the next cycle. To measure bond lifetime under zero force, we used the thermal fluctuation assay (8–10). The thymocyte cell was retracted to the null position to allow bond association and dissociation under zero force, which manifest as sudden reduction and resumption, respectively, in the thermal fluctuations of the bead. Thermal fluctuations were quantified by 100-point sliding SD (Fig. S13*D*) of the bead position (Fig. S13*C*) over time, which had a mean of 5 or 7 nm in the presence or absence of a bond. Lifetime was measured from the instant when SD of the position dropped below 5.0 nm to the instant that it rose above 5 nm.

To measure the molecular stiffness, we used previously described stretch method (8). The slope of the force vs. displacement curve is the stiffness of the system, including the cell and the molecular complex that were serially linked. As such, the reciprocal of the system stiffness, $1/k_{cell\text{-}mol}$, equals the sum of the reciprocals of the cellular and molecular stiffness, $1/k_{cell} + 1/k_{mol}$. By measuring the k_{cell} and $k_{cell\text{-}mol}$ form blue and red slopes, we can obtain the molecular stiffness.

Rap1/2 Activation Assay. Thymocytes were resuspended in serum-free OptiMEM I and incubated at 37 °C for 6 h to generate a low GTPase activation state. Following washing and resuspension at 4.4×10^7/mL, 10^7 cells (225 μL) at time 0 were transferred for each experimental condition to a microfuge tube incubating in a 37 °C water bath, and 25 μL of appropriate control medium, CXCL12 (final concentration 200 ng/mL) or CXCL12 with sema3E (final concentration 5 μg/mL), was added. After incubation at 37°C for 3 min, the cells were pelleted and washed twice in ice-cold Tris-buffered saline and resuspended in lysis buffer [500 μL; Triton X-100, 1%; deoxycholate, 1%; NaCl, 500 mM; Tris·HCl, 50 mM, pH 7.2; $MgCl_2$, 10 mM; protease inhibitors (no EDTA)] and incubated on ice with occasional agitation for 5 min.

Following clearing by centrifugation at 21,000 × *g* for 10 min, 50 μL was removed for use both as loading control and for protein assay, and the remaining 450 μL was rapidly snap-frozen in liquid N_2 and stored at −80°C until assayed. As a positive control, one sample was treated with 0.5 M EDTA (10 μL) and GTPγS (5 μL at 10 mM) was added. The positive control sample was incubated at 30°C for 30 min to load endogenous GTPases with GTPγS, after which the reaction was terminated by addition on ice of $MgCl_2$ (32 μL, 1 M; final concentration 60 mM). Subsequent to this point, the positive control was treated identically to the experimental sample lysates. Glutathione agarose beads (50% suspension in 50 μL lysis buffer) were preloaded with 30 μg of purified GST-Ral-GDS-RBD (plasmid kindly provided by V. Boussiotis, Beth Israel-Deaconess Hospital Medical Center, Boston, MA), washed, pelleted, and added to each thawed lysate. The samples were rotated end-over-end at 4 °C for 30 min and then washed four times with ice-cold lysis buffer. Following the final wash, residual liquid was removed using a gel loading tip, and 50 μL of 2× Laemmli SDS/PAGE buffer was added followed by separation on a 10% polyacrylamide gel and transfer to PVDF. After overnight blocking in TBS/BSA [5% (wt/vol)]/Tween 20 (0.5%), the blots were incubated overnight with a mix of antibodies against Rap1/Rap2 isoforms (1:200 in blocking buffer), and developed and imaged using anti-rabbit IgG-HRP and chemiluminescent reagents (Supersignal West Dura Extended Duration substrate; Thermo Scientific).

Autoantibody Analysis. Whole blood was collected from 4-mo-old mice. After incubating the blood at 37 °C for 1 h, the blood was spun down for 15 min at 12,000 rpm. The serum was collected and used for Western blotting at a 1:500 dilution.

Metabolic Parameter Determination. Fasting blood glucose was assayed in tail vein blood over a 6-wk period (mouse age: 14–16 wk) using a commercially available blood glucose meter and test

strips (OneTouch UltraMini; LifeScan), and body weight was determined simultaneously.

Statistical Analysis. Statistical analysis was performed using an unpaired, two-tailed Student *t* test unless otherwise specified. Nonnormally distributed data, e.g., cell velocities on exposure to sema3E, were compared using the Kolmogorov–Smirnov statistic. A probability level of $P < 0.05$ was considered statistically significant, and specific probabilities are presented in the text, figures, or their legends.

1. Choi YI, et al. (2008) PlexinD1 glycoprotein controls migration of positively selected thymocytes into the medulla. *Immunity* 29(6):888–898.
2. Kurts C, et al. (1996) Constitutive class I-restricted exogenous presentation of self antigens in vivo. *J Exp Med* 184(3):923–930.
3. Barnden MJ, Allison J, Heath WR, Carbone FR (1998) Defective TCR expression in transgenic mice constructed using cDNA-based alpha- and beta-chain genes under the control of heterologous regulatory elements. *Immunol Cell Biol* 76(1): 34–40.
4. Rasband WS (1997–2005) *ImageJ* (US National Institutes of Health, Bethesda, MD).
5. Vielkind S, Gallagher-Gambarelli M, Gomez M, Hinton HJ, Cantrell DA (2005) Integrin regulation by RhoA in thymocytes. *J Immunol* 175(1):350–357.
6. Yago T, et al. (2004) Catch bonds govern adhesion through L-selectin at threshold shear. *J Cell Biol* 166(6):913–923.
7. Rossy J, Owen DM, Williamson DJ, Yang Z, Gaus K (2013) Conformational states of the kinase Lck regulate clustering in early T cell signaling. *Nat Immunol* 14(1):82–89.
8. Chen W, Lou J, Evans EA, Zhu C (2012) Observing force-regulated conformational changes and ligand dissociation from a single integrin on cells. *J Cell Biol* 199(3):497–512.
9. Chen W, Zarnitsyna VI, Sarangapani KK, Huang J, Zhu C (2008) Measuring receptor-ligand binding kinetics on cell surfaces: From adhesion frequency to thermal fluctuation methods. *Cell Mol Bioeng* 1(4):276–288.
10. Chen W, Evans EA, McEver RP, Zhu C (2008) Monitoring receptor-ligand interactions between surfaces by thermal fluctuations. *Biophys J* 94(2):694–701.

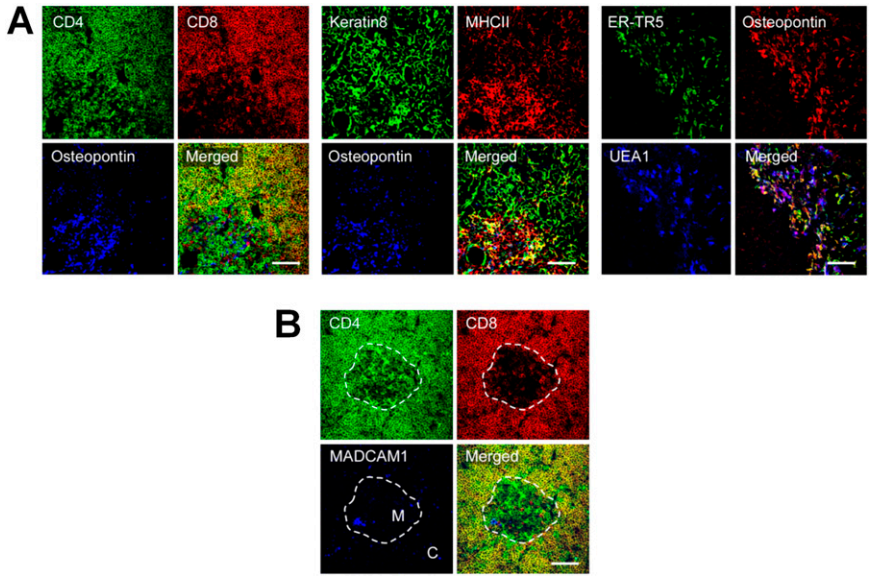

Fig. S1. Thymic expression of osteopontin and MAdCAM1. (*A*) Confocal analysis of frozen thymic sections demonstrates that osteopontin is not expressed in the cortex (coinciding with the yellow merged image for $CD4^+CD8^+$ DP thymocytes) but instead is expressed in the medullary region where MHC class II expression and the medullary markers UEA1 and with ER-TR5 are found. Note the strong colocalization of osteopontin with ER-TR5 labeling, raising the possibility that the target for ER-TR5, currently undefined, is osteopontin. (*B*) MAdCAM1, binding $\alpha4\beta7$, is minimally expressed in the thymus.

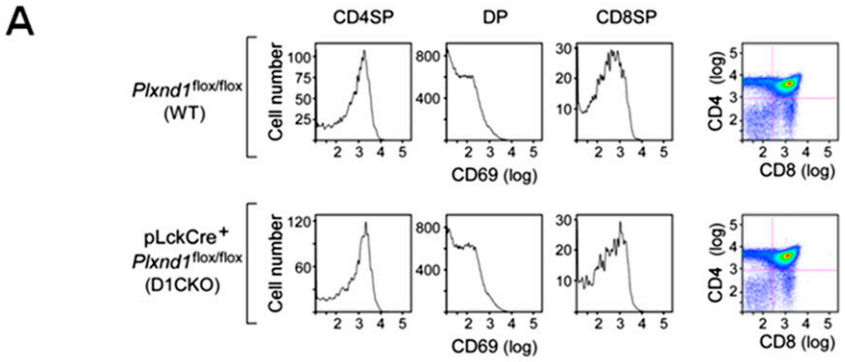

B

Integrin expression on thymocytes

Stage	β Integrin	α integrin	Possible combination
DP	β1, β2	α4, α6, αL	**α4β1, α6β1**, α4β2, α6β2, αLβ1, **αLβ2**
CD69+DP	β1, β2	α4, α6, αL	**α4β1, α6β1**, α4β2, α6β2, αLβ1, **αLβ2**
CD69+CD4SP	β1, β2, β3	α4, α5, α6, αL	**α4β1, α5β1, α6β1**, α4β2, α5β2, α6β2, α4β3, α5β3, α6β3, αLβ1, **αLβ2**, αLβ3
CD4SP	β1, β2, β3	α4, α5, α6, αL	**α4β1, α5β1, α6β1**, α4β2, α5β2, α6β2, α4β3, α5β3, α6β3, αLβ1, **αLβ2**, αLβ3
CD69+CD8SP	β1, β2, β3, β7	α4, α5, α6, αL	**α4β1, α5β1, α6β1**, α4β2, α5β2, α6β2, α4β3, α5β3, α6β3, **α4β7**, α5β7, α6β7, αLβ1, **αLβ2**, αLβ3, αLβ7
CD8SP	β1, β2, β3, β7	α4, α5, α6, αL	**α4β1, α5β1, α6β1**, α4β2, α5β2, α6β2, α4β3, α5β3, α6β3, **α4β7**, α5β7, α6β7, αLβ1, **αLβ2**, αLβ3, αLβ7

Identified Ligands of integrins on thymocytes

α4β1: VCAM1, Osteopontin, Thrombospondin, Fibronectin
α4β7: VCAM1, Osteopontin, Fibronectin, MADCAM1
α6β1: Laminin
α5β1: Osteopontin, Fibronectin
αLβ2: ICAM1

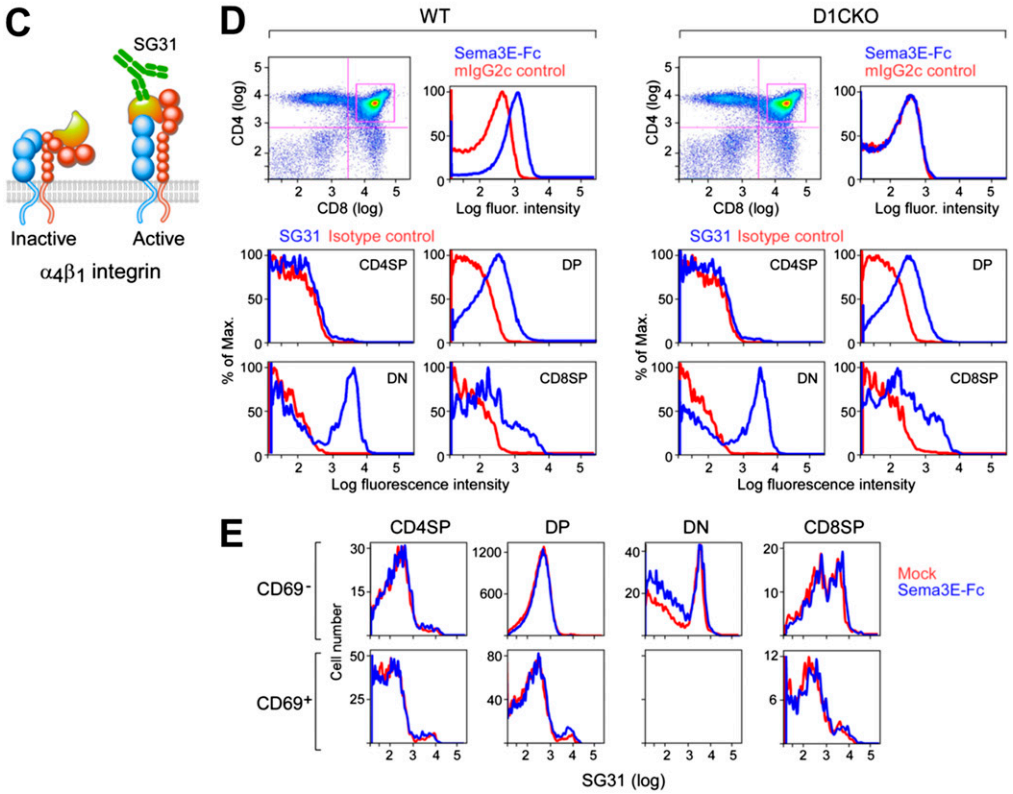

Fig. S2. Developing thymocytes from WT and D1CKO mice exhibit similar CD69$^+$ expression and similar total integrin and activated α4 integrin profiles. (*A*) After gating based on CD4 and CD8 expression, the DP, CD4$^+$ SP, and CD8$^+$ SP thymocytes were stained for anti-CD69 and analyzed by flow cytometry. (*B*) Based on the results shown in Fig. S3, thymocytes differentiating from the DP stage onwards were observed to express the indicated α and β integrins. As obligate heterodimers, for each cell subtype, several combinations of α and β integrin may form where the known heterodimers are expressed in bold red type. For the known heterodimers (α4β1, α4β7, α6β1, α5β1, and αLβ2) implied by our analysis to be expressed on thymocytes, the currently defined ligands are listed. (*C*) SG31 mAb specifically recognizes an active conformation of the α4 integrin (1). The β chain is in red and the α chain in orange and blue. For simplicity only,

Legend continued on following page

bent and fully extended α4β1 conformers are depicted. (*D*) Gating on the DP thymocytes, plexinD1 was detected by binding of sema3E-Fc to WT and D1CKO cells confirming loss of plexinD1 in the latter. Gated subsets were assessed for activated α4 integrin expression using the SG31 mAb. (*E*) WT thymocytes were incubated with or without sema3E-Fc and gated subpopulations examined for SG31-binding. The blue lines represent reactivity of sema3E-treated WT thymocytes, whereas the red lines represent activity of mock-treated (mFc only exposed) WT thymocytes.

1. Shu F, Holzmann B, Seibold F, Erle D, Kearney JF (2002) Activated alpha4 integrins are preferentially expressed on immature thymocytes and activated T cells. *Dev Immunol* 9(2):73–84.

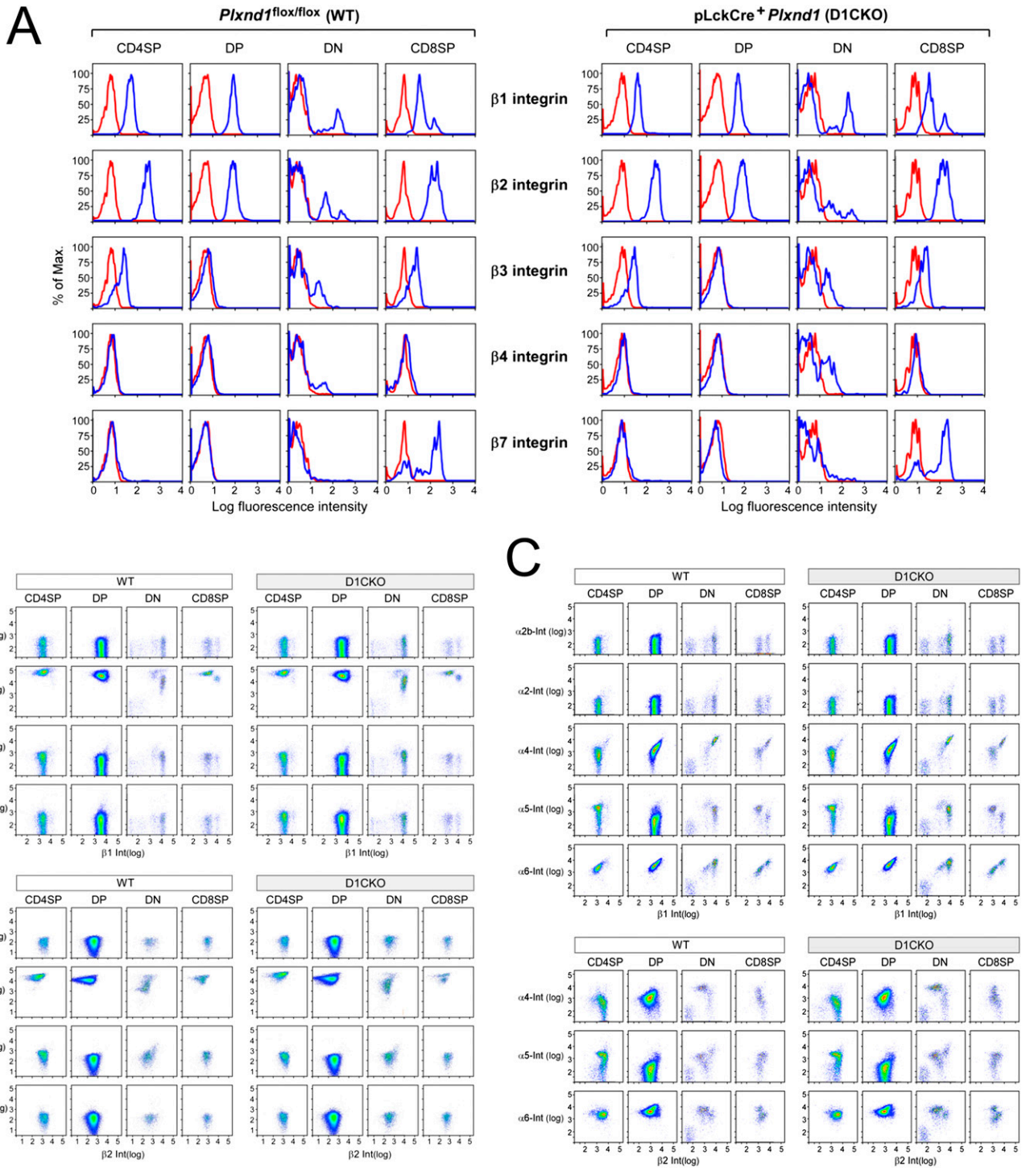

Fig. S3. Integrin expression on thymocytes. Thymocytes from the WT or D1CKO B6 mice were stained with the indicated chain-specific integrin antibodies and analyzed by flow cytometry. (*A*) After gating subpopulations based on anti-CD4 and anti-CD8 staining, overall β integrin expression was compared as histograms between WT and D1CKO thymocytes using specified antibodies (blue) and isotype controls (red). (*B* and *C*) Designated α integrins are shown together with β1 or β2 integrins as dot plots to characterize potential αβ integrin heterodimers on thymocytes.

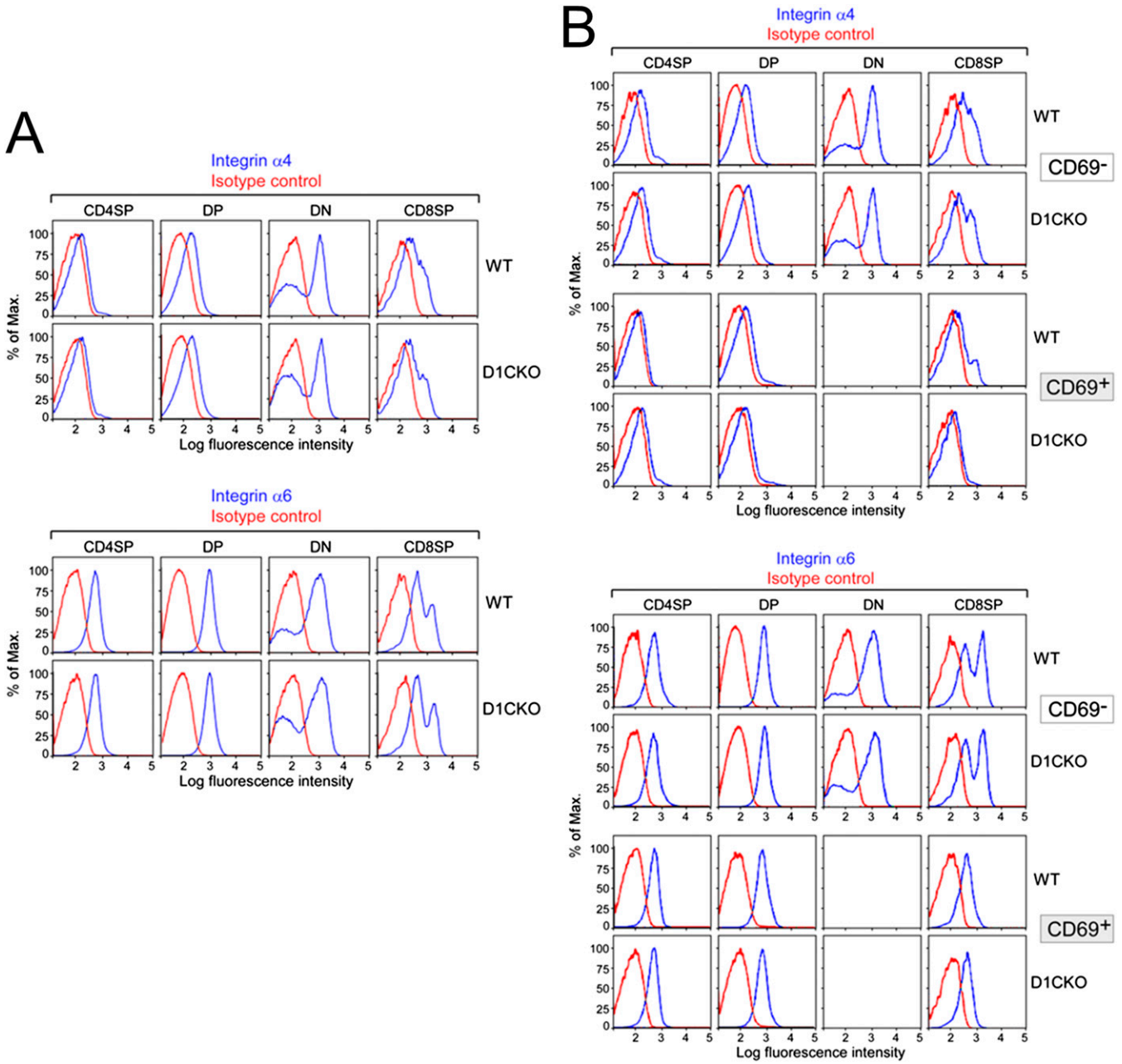

Fig. S4. α4 and α6 integrin profiles are identical on WT and D1CKO thymocytes. (*A*) Thymocyte subsets were labeled with α4 or α6 integrin-specific antibodies, incubated with flurophore-labeled secondary reagents and analyzed by flow cytometry. (*B*) Similar analysis of gated $CD69^+$ and $CD69^-$ populations was also analyzed for α4 and α6 integrin expression. Note that because CD69 is not expressed on DN cells, this population could not be analyzed.

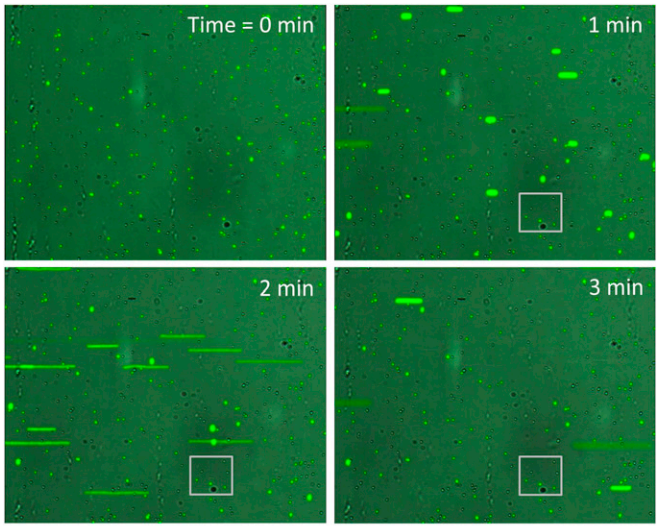

1st 4 frames of movieS1.mov

Fig. S5. Adhesion of WT and D1CKO thymocytes to VCAM-1: analysis immediately after initiation of flow. This figure presents the WT (unlabeled) and D1CKO (green) thymocyte movement over the first 3 min of Movie S1. At time = 0, the cells had been incubating for 30 min at 37 °C on the VCAM-1 surface, following which flow was initiated at ∼2–4 μL/min from the left. Note that flow dislodges a large number of D1CKO cells, some traversing the chamber quickly, others rolling on the surface, such that by 3 min the initial 1:1 ratio of WT:D1CKO cells is now considerably altered. As a point of reference, the gray outlined box identifies three WT and three D1CKO cells that remain adherent.

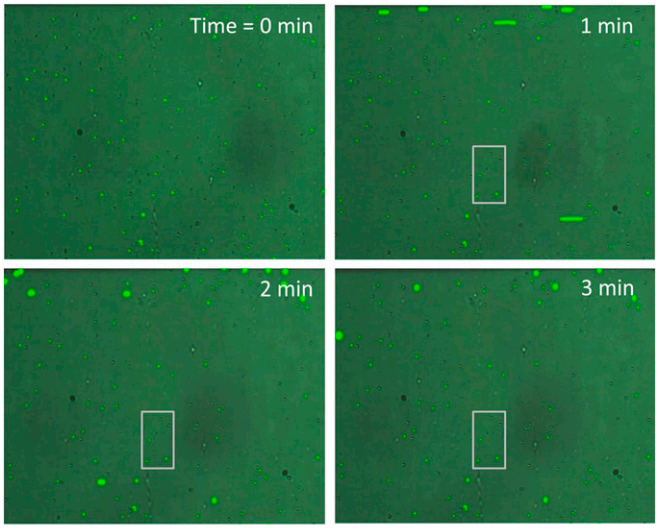

1st 4 frames of movieS2.mov

Fig. S6. Adhesion of WT and D1CKO thymocytes to laminin: analysis immediately after initiation of flow. This figure presents the WT (unlabeled) and D1CKO (green) thymocyte movement over the first 3 min of Movie S2. At time = 0, the cells had been incubating for 30 min at 37 °C on the laminin surface following which flow was initiated at ∼2–4 μL/min from the left. Note that flow preferentially dislodges D1CKO cells but that the ratio of adherent WT to D1CKO cells at 3 min is not significantly altered (as presented in Fig. 2*A*, *Right*). As a point of reference, the gray outlined box identifies three WT and three D1CKO cells that remain adherent.

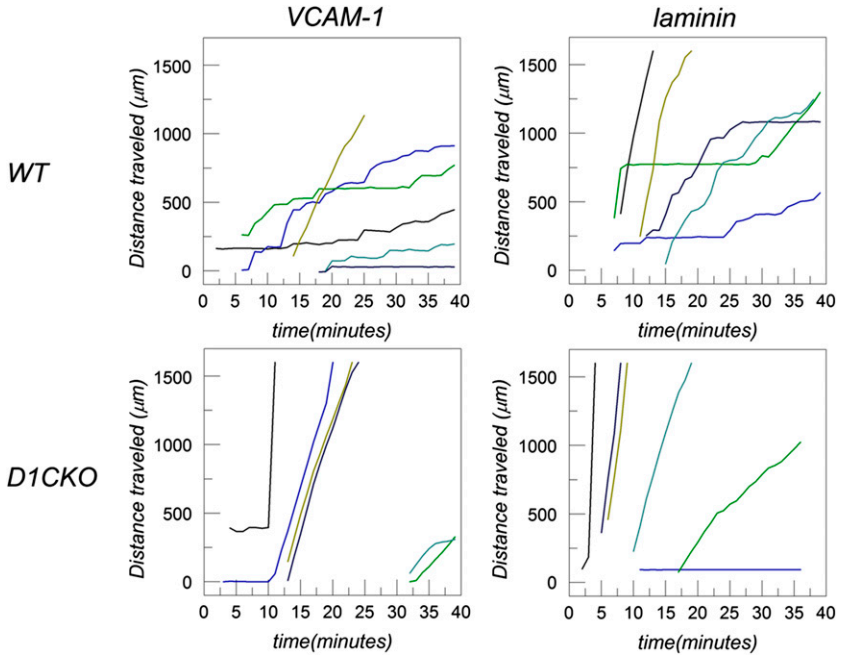

Fig. S7. WT and D1CKO do not move identically under flow on VCAM-1 or laminin-coated surfaces. As depicted in Fig. 2*A*, some cells are not dislodged immediately from the surface following adherence but move on the surface in the direction of the applied flow pressure gradient. For each condition, the movement of six such cells, representing the full range of behaviors observed, is presented. On the abscissa is the time after application of flow that a cell began to move. On the ordinate is represented the cumulative distance traveled over the indicated time period. Note that the WT cells on either VCAM-1 or laminin exhibit a consistent adherent phase followed by a short phase of movement and repetition of this cycle leading to a stepwise appearance to the profile. In contrast, the D1CKO cells exhibit no static adherent phase and roll across either surface.

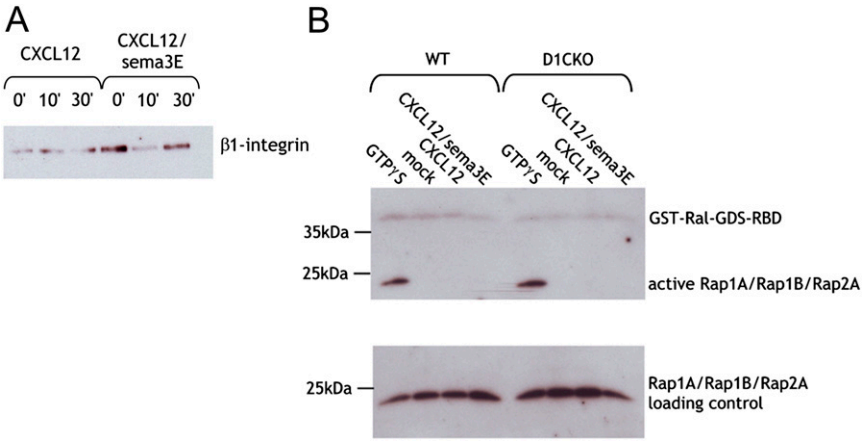

Fig. S8. Sema3E does not regulate integrin avidity by affecting endocytotic recycling, and Rap1 signaling upstream of integrin activation is identical between WT and D1CKO cells independent of sema3E. (*A*) WT thymocytes were surface labeled with a thiol-linked biotin adduct, stimulated as indicated and then surface, noninternalized biotin removed by disulphide-bond reduction and blocking of exposed free –SH with iodoacetamide. Biotin in the lysates then represents material internalized from the surface. Following immunoprecipitation of the biotin-labeled protein with streptavidin beads, detection of β1 integrin reveals no significant difference in internalization between control and sema3E-incubated conditions (representative of five experiments). Further, in all experiments, signal development was extended due to the very low amounts internalized by the thymocytes. (*B*) The Rap1 and Rap2 proteins have been identified as central mediators of integrin activation following extracellular stimulation. Following 30-min incubation with CXCL12 (200 ng/mL) with or without sema3E (5 μg/mL), no pulldown of active Rap1/Rap2 by GST-Ral-GDS-RBD is observed (*Upper*). (*Lower*) Rap1/2 signal from 5% of starting lysate. The positive controls in the upper panel consist of spiking lysate with GTPγS. The GTPγS maintains Rap1/2 GTPases in the active state because it is not susceptible to hydrolysis by the autocatalytic activity of the activated GTPases.

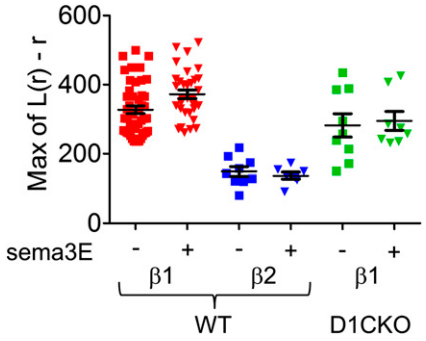

Fig. S9. Sema3E does not affect β1 integrin clustering on D1CKO cells. Degree of clustering of β1 integrin, assessed by the *Max of L*(*r*) − *r* parameter, confirms that sema3E treatment of D1CKO does not alter the nanoscale individual molecular distribution on the thymocyte surface detected by direct stochastic optical reconstruction microscopy (dSTORM). The clustering data for β1 and β2 integrins on WT cells are included for comparative purposes.

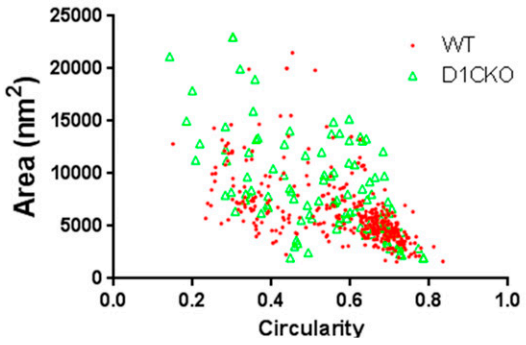

	Area		Circularity	
	Mean ± SEM	P	Mean ± SEM	P
β1 WT N=436	6498 ± 153	$<10^{-4}$	0.5539 ± 0.0074	0.084
β1 D1CKO N=132	8219 ± 394		0.5267 ± 0.0138	

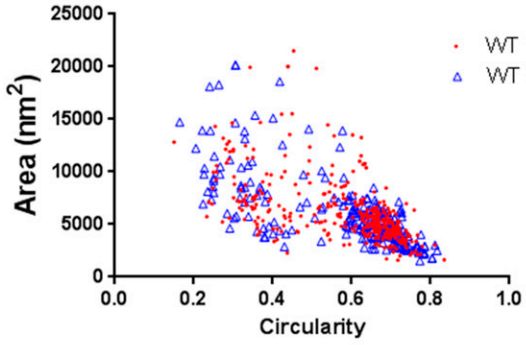

	Area		Circularity	
	Mean ± SEM	P	Mean ± SEM	P
β1 WT N=436	6498± 153	0.50	0.5539 ± 0.0074	0.66
β1 WT + sema3E N=299	6329 ± 196		0.5483 ± 0.0104	

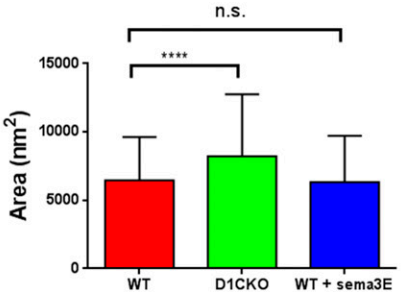

Fig. S10. Absence of plexinD1 leads to less constrained membrane clustering of β1 integrins, an effect not recapitulated by sema3E binding. Morphological analysis of the individual cluster representations in Fig. 3*E* demonstrate that, in the absence of plexinD1 in D1CKO cells (*Upper*, green triangles), the area of the β1 clusters significantly increases in comparison with WT thymocytes (red dots). Addition of sema3E (*Lower*, blue triangles) has no effect on this parameter. These results are summarized in the bar graph. Circularity, calculated as $4\pi(\text{area}/\text{perimeter}^2) = 1$ for a perfect circle. The circularity of the D1CKO clusters displays a larger area distribution with less homogenous shape. β2 integrin clusters, due to low density and amorphous shape, were not dense enough to be detected by this morphological analysis.

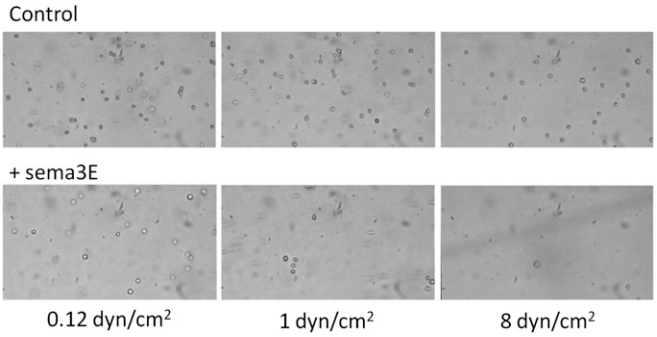

Fig. S11. Representative images of rolling adherent cells in parallel flow chamber under increasing shear force. The shear forces represent three differing wall shear stress conditions contributing to Fig. 4*E*. In the control condition, WT thymocytes perfusing over a VCAM-1–coated surface, the number of adherent cells rolling increased with wall shear stress from 0.12 to 1 dyn/cm^2, and then decreased as the wall shear stress increased from 1 to 8 dyn/cm^2. By comparison, the number of sema3E-treated WT thymocytes adherent to the VCAM-1 surface decreased as the wall shear stress increased from 0.12 through 1–8 dyn/cm^2 and was lower than the untreated values at each of the corresponding wall shear stresses.

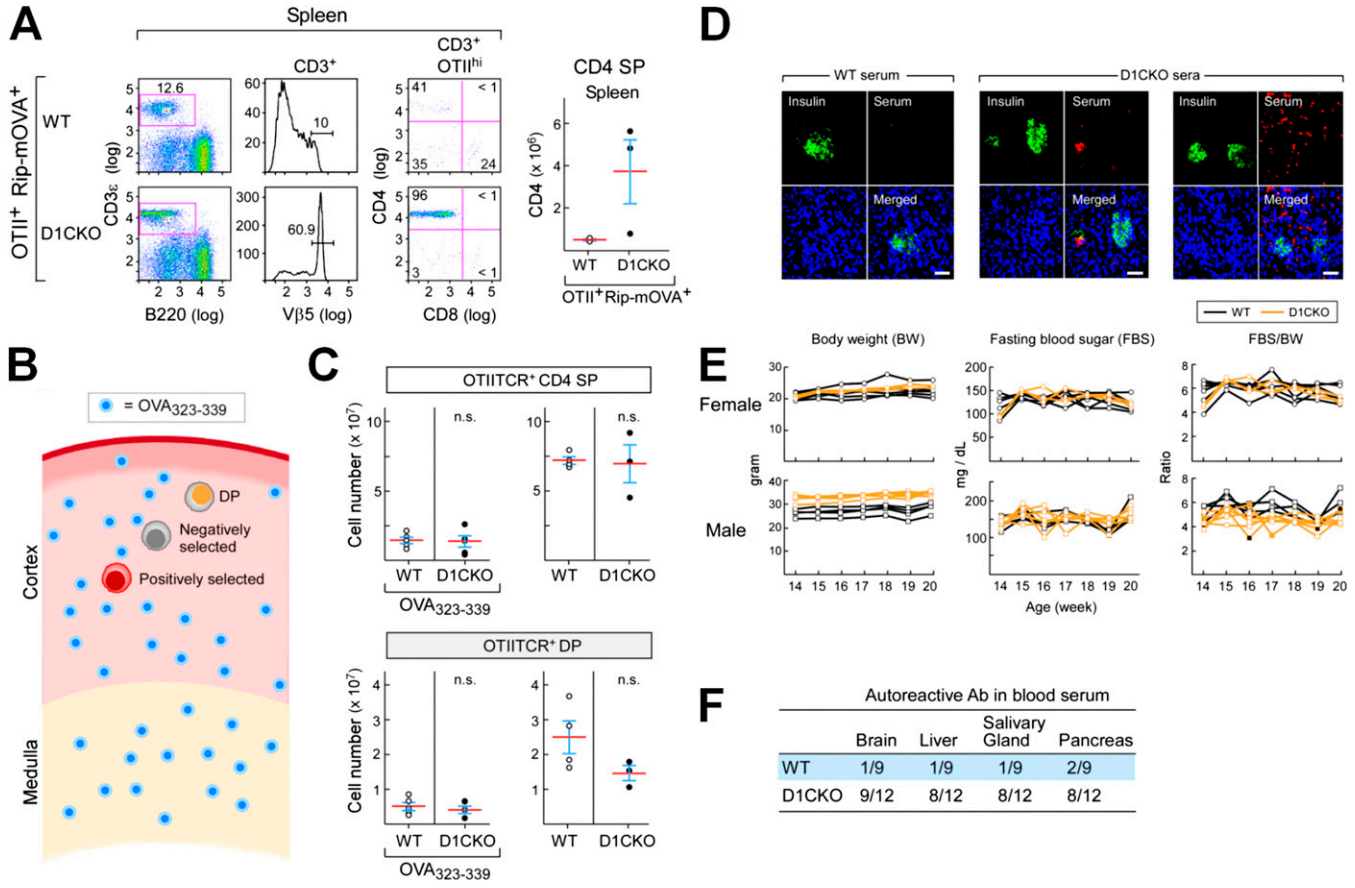

Fig. S12. Failure of negative selection in D1CKO mice reflected in the periphery; migration-independent negative selection is normal in D1CKO mice; and development of anti-pancreas and other tissue autoantibodies without overt symptoms of autoimmune diseases. (*A*) The mature OTII TCR^{hi} T-cell population from spleen was analyzed by FACS demonstrating the high survival of CD3$^+$ OTII TCR^{hi} CD4 SP cells, confirming the results shown for similar cells in the lymph node (Fig. 5 *C* and *D*). The difference between WT and D1CKO absolute number of CD4 SP cells was statistically significant ($P = 0.042$). (*B*) i.v. peptide injection diffusely distributes an epitope throughout the thymus evenly so that thymocytes are not required to migrate to the medulla for OVA peptide scanning. (*C*) To induce the negative selection of OTII TCR$^+$ thymocytes, $OVA_{323–339}$ peptide (50 μg in PBS) was injected twice at day −5 and day −1. At day 0, thymocyte single cell suspensions were prepared and analyzed as described previously (1). The reduction of thymic cellularity was similar between WT and D1CKO mice (n.s. = not significant). (*D*) D1CKO antisera containing substantial autoantibody titers were used to stain pancreatic tissue sections of *Rag2*$^{-/-}$ mice (1:500) using anti-insulin Ab to visualize the β islets. Note that the D1CKO serum reactivity is not directed against the insulin-containing islets. The white bar in the merged image represents 100 μm. (*E*) Supporting the lack of reactivity to β islets, fasting blood sugar and body weight measurements over a 7-wk period indicate no significant variation of D1CKO from WT for either parameter. Each line represents one mouse. (*F*) Tabulation of autoantibody activity detected in WT vs. D1CKO mouse sera.

1 Choi YI, et al. (2008) PlexinD1 glycoprotein controls migration of positively selected thymocytes into the medulla. *Immunity* 29(6):888–898.

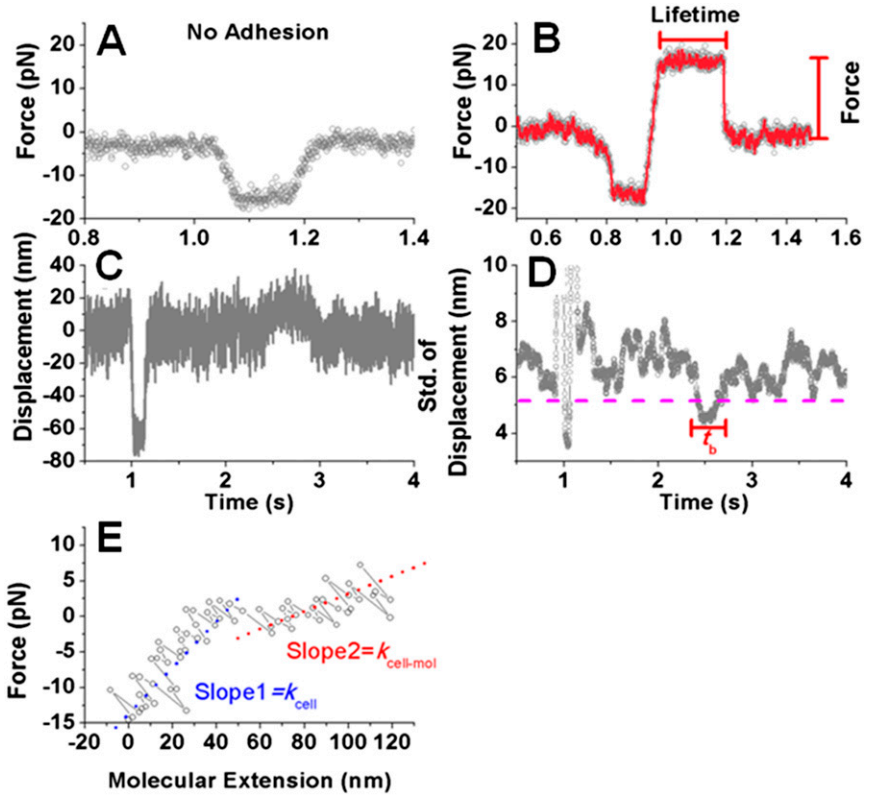

Fig. S13. Example of processing of BFP contributing to Fig. 4 *B* and *C*. Representative raw data of force vs. time curves of the force-clamp assay showing (*A*) a contact cycle without an adhesion event; (*B*) another cycle with an adhesion event followed by a surviving lifetime; (*C*) raw data of displacement vs. time curve; and (*D*) 100-point sliding SD (*Std*) of displacement vs. time curve of the thermal fluctuation assay. Lifetimes in *B* and *C* are indicated. Bond formation and dissociation in *C* are identified, respectively, by the reduction of the *Std* below, and its resumption above, a threshold indicated by the pink horizontal dashed line. (*E*) Representative raw data of force vs. molecular extension curve. Slope1 (blue dashed line) depicts cellular stiffness k_{cell}, and slope 2 (red dashed line) represents system stiffness ($k_{cell\text{-}mol}$) consisting of the cellular spring and molecular spring in series. Molecular stiffness of the α4β1/VCAM-1 complex was calculated by $k_{mol} = 1/(1/k_{cell-mol} - 1/k_{cell})$.

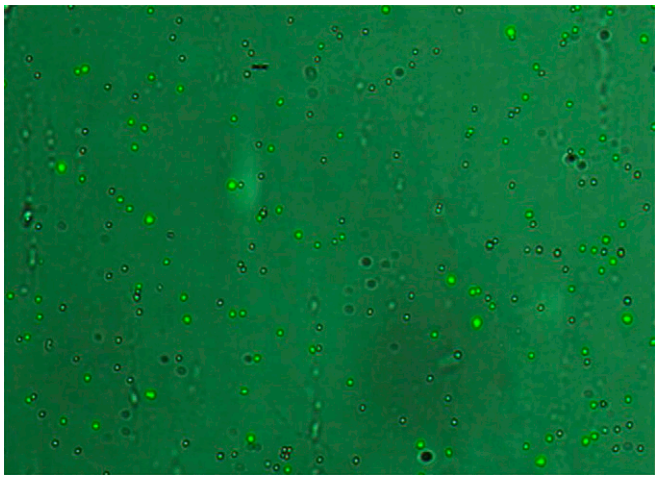

Movie S1. WT and D1CKO cells under flow on a VCAM-1 surface. This movie presents the data contributing to the left panels of Fig. 2*A*. WT (unlabeled) and D1CKO (BCECF/AM labeled; green) thymocytes were mixed 1:1, and CXCL12 was added, loaded into the VCAM-1–coated microfluidic chamber, and allowed to adhere for 30 min, followed by application of flow from left to right with imaging for 40 min.

Movie S1

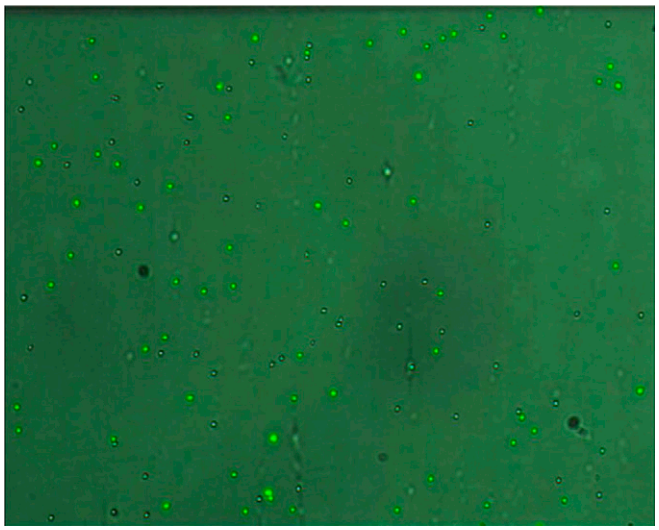

Movie S2. WT and D1CKO cells under flow on a laminin surface. This movie presents the data contributing to the right panels of Fig. 2*A*. WT (unlabeled) and D1CKO (BCECF/AM labeled; green) thymocytes were mixed 1:1, and CXCL12 was added, loaded into the laminin-coated microfluidic chamber, and allowed to adhere for 30 min, followed by application of flow from left to right with imaging for 40 min.

Movie S2

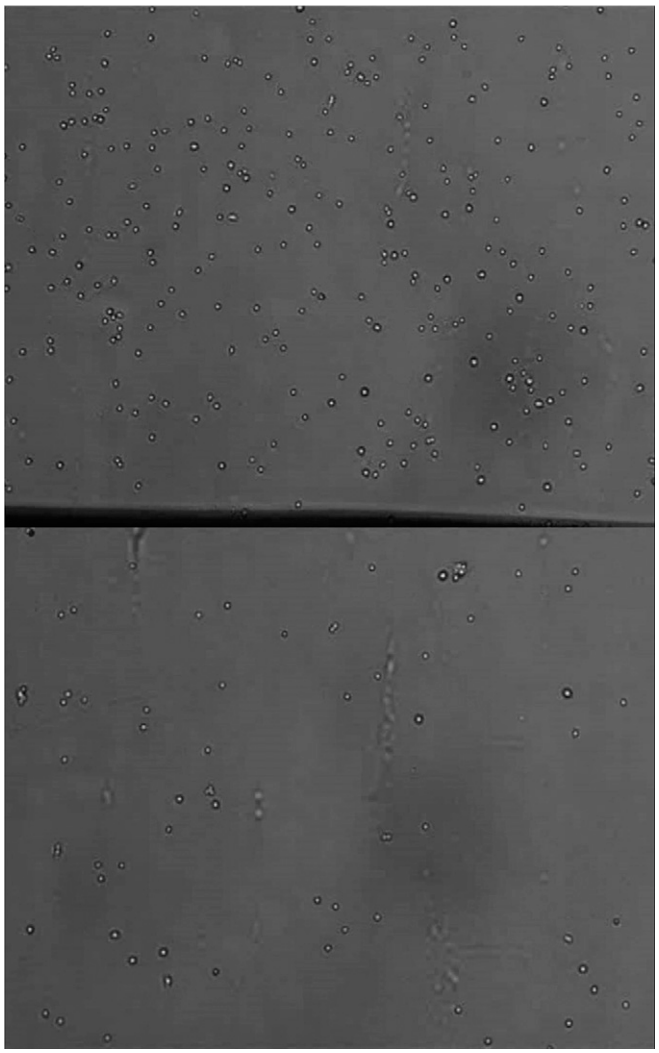

Movie S3. Effect of sema3E on WT adhesion under flow to VCAM-1. This movie presents the data contributing to the left panel of Fig. 2*B*. WT thymocytes (*Upper*) and WT thymocytes treated with sema3E (*Lower*) were simultaneously imaged following adherence to a VCAM-1–coated surface followed by application of flow in a left-to-right direction for 40 min.

Movie S3

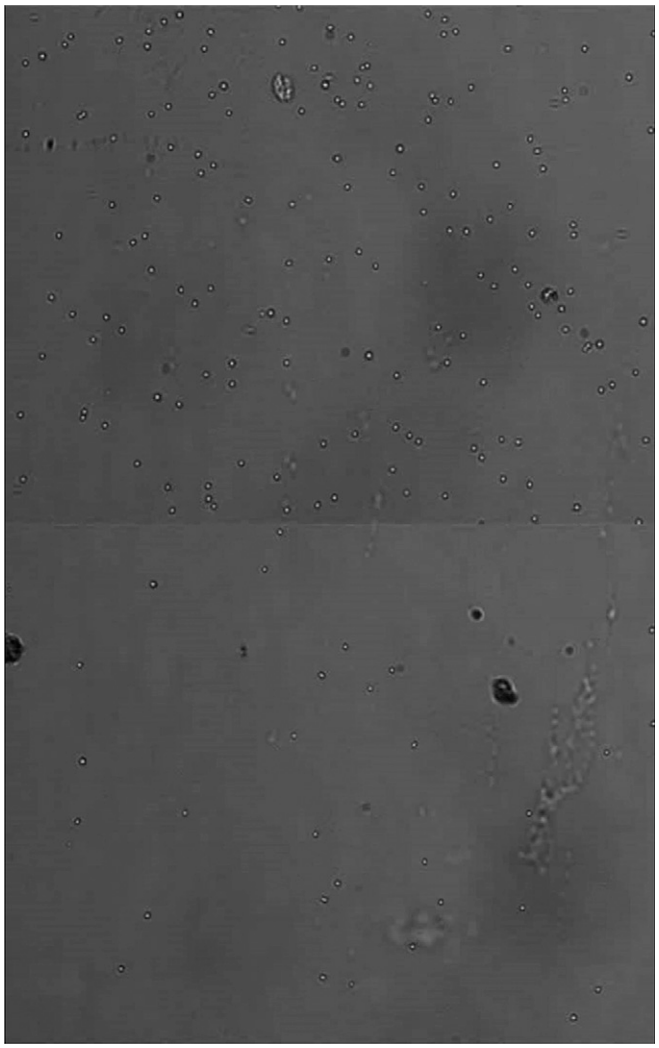

Movie S4. Effect of sema3E on WT adhesion under flow to laminin. This movie presents the data contributing to the right panel of Fig. 2*B*. WT thymocytes (*Upper*) and WT thymocytes treated with sema3E (*Lower*) were simultaneously imaged following adherence to a laminin-coated surface followed by application of flow in a left-to-right direction for 40 min.

Movie S4

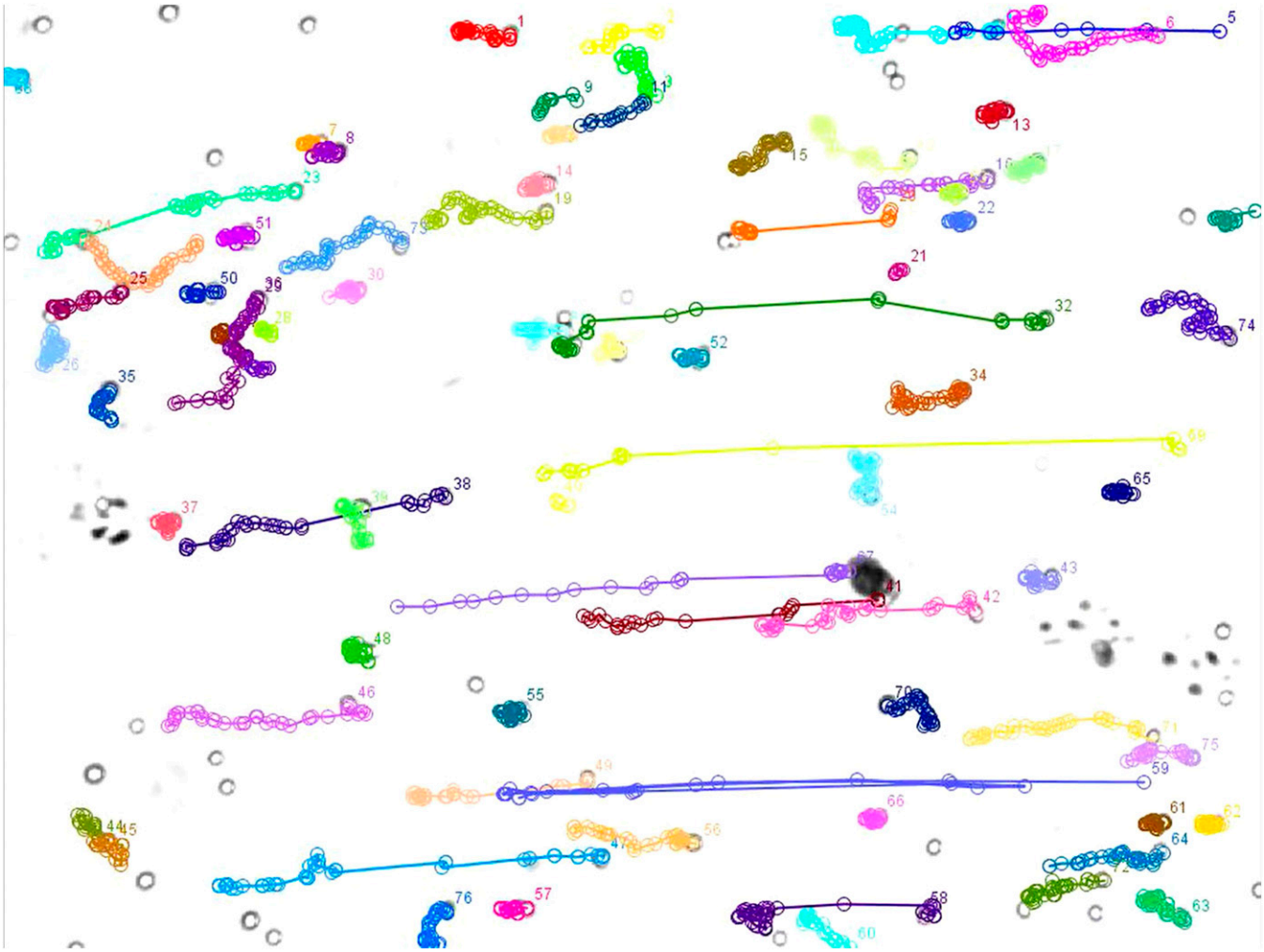

Movie S5. D1CKO thymocyte adherence to VCAM-1 under flow. D1CKO thymocytes were allowed to settle and adhere to a VCAM-1 surface for 30 min (time = 00:00–00:03 in movie) at 37 °C. At t = 00:03, flow was induced from left to right at ~3 μL/min. Individual cells observed to be adherent 1 min after flow initiation were then tracked for 40 min (t = 00:031–00:07) using the MTrackJ plugin for ImageJ. Note that a subpopulation of cells remain firmly adherent, exhibiting behavior characteristic of WT cells (e.g., tracks 48, 52, and 55) but that the majority of cells exhibit weakened adhesion and roll with the flow.

Movie S5

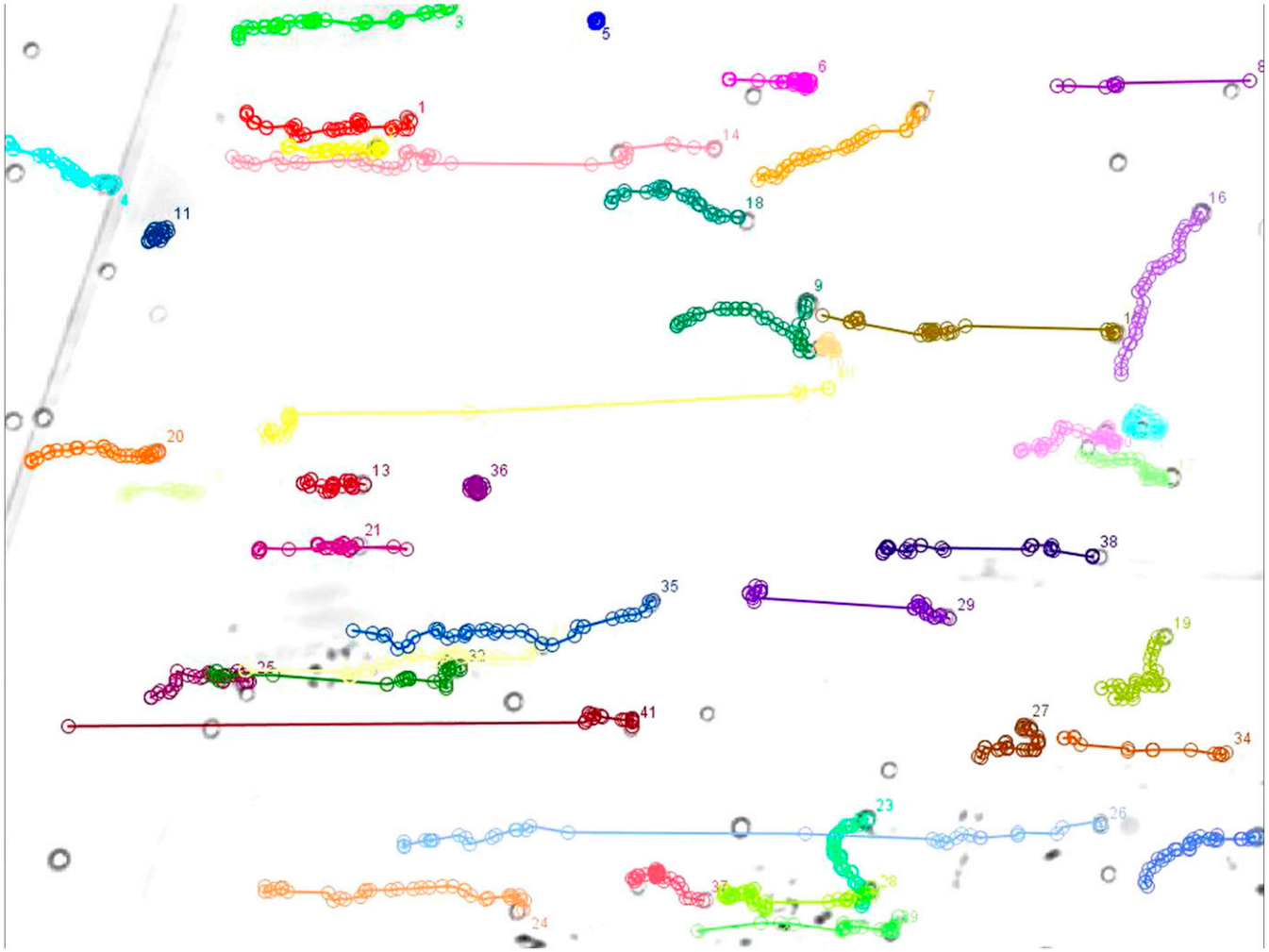

Movie S6. D1CKO thymocyte adherence to VCAM-1 under flow and in the presence of sema3E. This movie depicts an experiment identical to that described above for Movie S5 except that the thymocytes are continuously exposed to sema3E (5 μg/mL). Under these circumstances, the behavior of the cells is identical to that observed in the absence of sema3E.

Movie S6

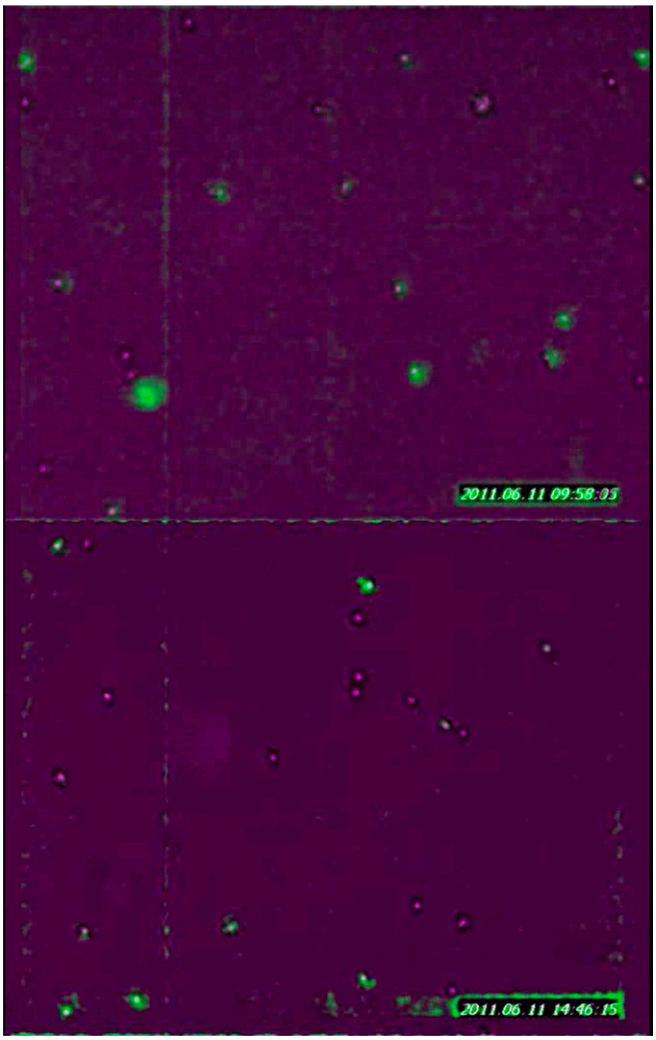

Movie S7. WT and D1CKO chemokine-driven migration on control and VCAM-1–coated surfaces. This movie presents the data contributing to the top two panels of Fig. 2C. WT (unlabeled) and D1CKO (BCECF/AM-labeled; green) thymocytes were imaged while responding to a CXCL12 gradient emanating from the right on a control untreated surface (*Upper*) or a VCAM-1–coated surface (*Lower*).

Movie S7

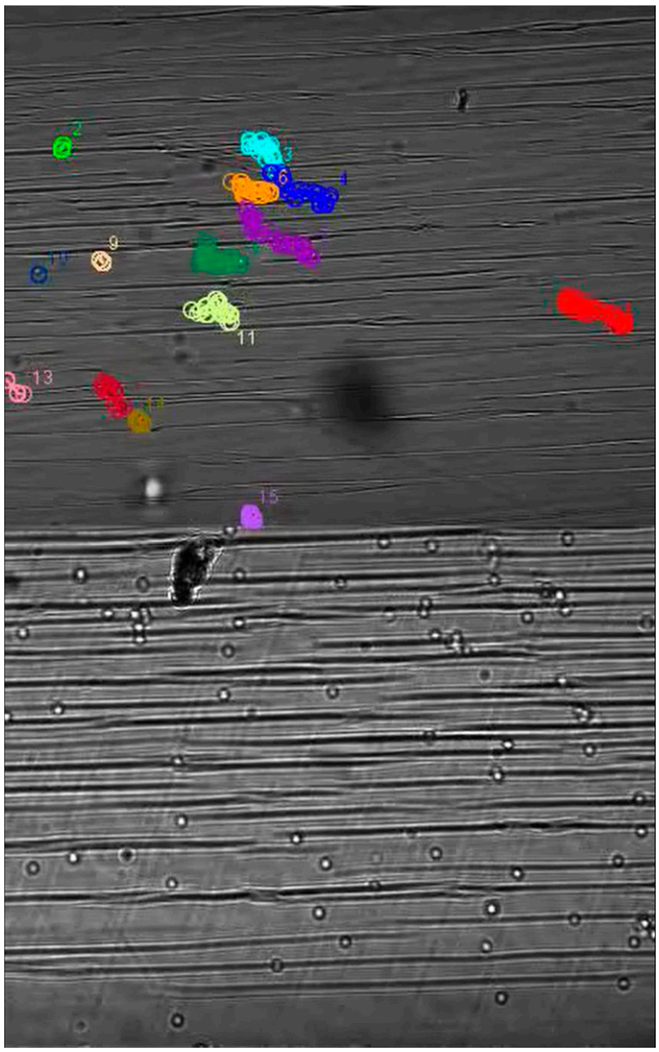

Movie S8. Tracking of chemokine-driven individual untreated WT thymocytes migrating on VCAM-1. This movie presents the data contributing to the lower left panel of Fig. 2*C* depicting migration on a VCAM-1–coated surface of untreated WT (*Upper*) and sema3E-treated WT (*Lower*) thymocytes imaged while responding to a CXCL12 gradient emanating from the right. The positions of the untreated WT cells as they respond to the chemokine gradient over time are tracked using the MTrackJ plugin for ImageJ (*Upper*; one color per cell).

Movie S8

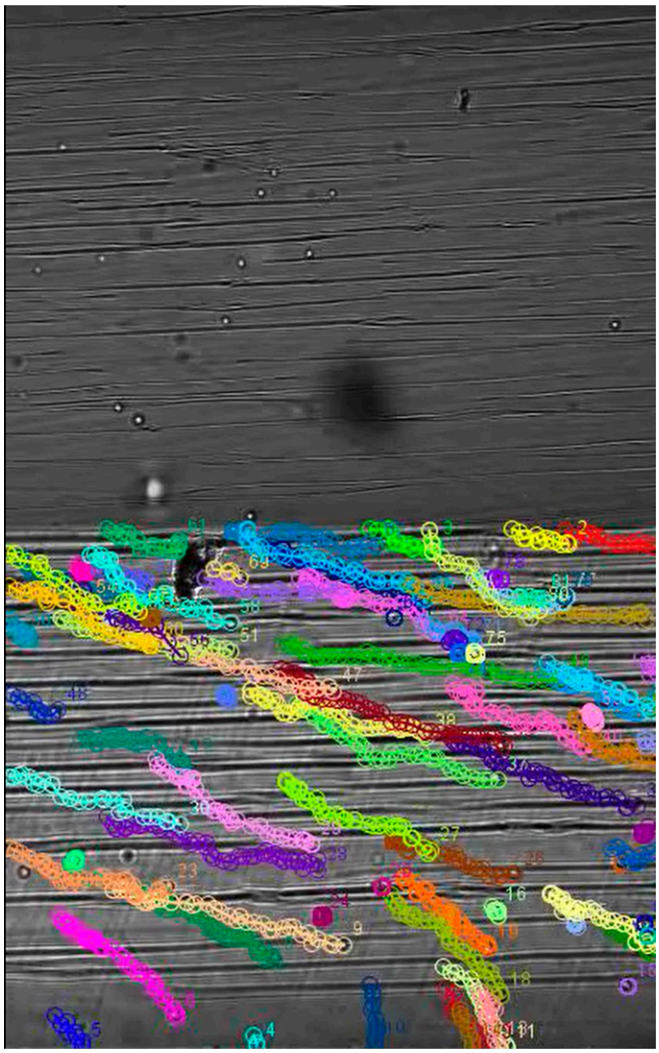

Movie S9. Tracking of chemokine-driven individual sema3E-treated WT thymocytes migrating on VCAM-1. This movie presents the data as in Movie S8, instead tracking the migration path for each sema3E-treated WT cell responding to CXCL12 using the MTrackJ plug-in module for the ImageJ package (*Lower*; one color per cell).

Movie S9